



Exploring the inhibitory potential of xanthohumol on MEK1/2: a molecular docking and dynamics simulation investigation

Zohreh Gholizadeh Siahmazgi¹, Shiva Irani², Ali Ghiaseddin³, Fereshteh Soutodeh⁴, Zahra Gohari⁴, Jaber Afifeh¹, Amirreza Pashapouryeganeh¹, Hilda Samimi¹, Mahmood Naderi⁵, Parviz Fallah^{6,*}, and Vahid Haghpanah^{1,7,*}

¹Endocrinology and Metabolism Research Center, Endocrinology and Metabolism Clinical Sciences Institute, Tehran University of Medical Sciences, Tehran, I.R. Iran.

²Department of Biology, Science and Research Branch, Islamic Azad University, Tehran, I.R. Iran.

³Department of Biomedical Engineering Division, Chemical Engineering Faculty, Tarbiat Modares University, Tehran, I.R. Iran.

⁴Department of Molecular Biology and Genetic Engineering, Stem Cell Technology Research Center, Tehran, I.R. Iran.

⁵Digestive Diseases Research Center, Digestive Diseases Research Institute, Tehran University of Medical Sciences, Tehran, I.R. Iran.

⁶Laboratory Science Department, Allied Medicine Faculty, Alborz University of Medical Sciences, Karaj, I.R. Iran.

⁷Personalized Medicine Research Center, Endocrinology and Metabolism Clinical Sciences Institute, Tehran University of Medical Sciences, Tehran, I.R. Iran.

Abstract

Background and purpose: Xanthohumol (Xn), a small molecule found in *Humulus lupulus*, has shown promise as an anti-cancer compound. This in silico study was performed to understand the mechanism of action of Xn as a natural compound on MEK1/2 by simulation.

Experimental approach: After ligand and protein preparation, the best binding energy was determined using Autodock 4.2. Additionally, molecular dynamics simulations of the MEK1/2-Xn and BRaf-MEK1/2-Xn complexes were conducted using GROMACS 2022.1 software and compared to the complexes of MEK1/2-trametinib (Tra) and BRaf-MEK1/2-Tra.

Findings/Results: The docking results revealed that the best binding energies for MEK1-Xn (-10.70 Kcal/mol), MEK2-Xn (-9.41 Kcal/mol), BRaf-MEK1-Xn (-10.91 Kcal/mol), and BRaf-MEK2-Xn (-8.54 Kcal/mol) were very close to those of the Tra complexes with their targets, MEK1 and MEK2. Furthermore, Xn was found to interact with serine 222 at the active site of these two kinases. The results of the molecular dynamics simulations also indicated that Xn induced changes in the secondary structure of the studied proteins. The root mean square of proteins and the mean radius of gyration showed significant fluctuations.

Conclusion and implications: The findings of the study suggested that Xn, as a novel bioactive compound, potentially inhibits the MEK1/2 function in cancer cells.

Keywords: Active site; MEK1; MEK2; Molecular dynamic simulation; Xanthohumol.

INTRODUCTION

The mitogen-activated protein kinase (MAPK) signaling pathway encompasses a group of protein kinases that play a pivotal role in cell growth, survival, differentiation, and angiogenesis. Defects in this pathway are observed in numerous human cancers (1).

Studies have suggested that this signaling pathway could serve as a target for drug interventions in cancer types characterized by uncontrolled cell proliferation (2).

*Corresponding authors:

V. Haghpanah, Tel: +98-2188220037-8, Fax: +98-2188220052

Email: v.haghpanah@gmail.com, vhaghpanah@tums.ac.ir

P. Fallah, Tel: +98-2632563318, Fax: +98-2632558920

Email: parvizfallah@gmail.com

Access this article online



Website: <http://rps.mui.ac.ir>

DOI: 10.4103/RPS.RPS_38_24

The MEK family comprises key enzymes in the MAPK signaling pathway. MEK1 and MEK2 are protein kinases with dual specificity, phosphorylating both serine/threonine and tyrosine residues of the extracellular signal-regulated kinase (ERK) downstream in the signaling pathway (1). The overexpression of the MEK1 gene in various cancer types is often attributed to the activation of the V-Raf murine sarcoma viral oncogene homolog B1 (BRAF)/MEK/ERK pathway by upstream kinases, growth factor receptors, and other unknown mechanisms (2).

The advantage of targeting the BRAF/MEK/ERK cascade is that it can be targeted without detailed knowledge of the genetic mutations that lead to unconventional pathway activation (3).

Trametinib (Tra) was the first MEK1/2 inhibitor approved by the United States Food and Drug Administration (4). The inhibitor can be utilized as a single or combination therapy to inhibit the MAPK signaling pathway in cancer treatment (5). Since MEK inhibitors are allosteric suppressors (non-competitors of ATP), they are expected to act more specifically than other kinases, potentially leading to increased clinical efficiency in patients (6). Therefore, inhibiting the BRAF/MEK/ERK pathway with MEK1/2 inhibitors could be a clinical advantage for cancer patients with anomalies in the MAPK pathway (7).

Over the past 2 decades, the small molecule xanthohumol (Xn) has been widely studied for its anticancer properties. Xn is one of the main active pharmaceutical ingredients in *Humulus lupulus* and is a prenylated flavonoid. It is extracted from the female flowers of *Humulus lupulus*, comprising 0.1 - 1% of the dry weight of plant (8). Recent research has shown that Xn has anticancer activities against various cancers, including lung, breast (9), glioblastoma, pancreas, thyroid, melanoma, uterus, ovary, and colon cancers (10). Considering the pivotal role of the MAPK pathway in many cancers and the significance of MEK1/2 in targeted therapy (10) and molecular docking and molecular dynamics (MD) simulations critical role in drug discovery by enabling the analysis of biological data, identification of drug targets, virtual screening of potential compounds, understanding disease

mechanisms, and optimizing drug development processes (11), this study employed molecular docking and MD simulations to compare the effects of Xn on MEK1 and MEK2 with those of Tra. For this purpose, MEK1/2-ATP proteins and BRAF-MEK1/2-ATP complexes were chosen as receptors, with Xn and Tra selected as ligands. The objective of this study was to propose Xn as a potential MEK1/2 inhibitor candidate and to gain a deeper understanding of the structural changes in MEK1 and MEK2 during interaction with Xn for future investigations.

MATERIALS AND METHODS

Molecular docking

To predict the ligand attachment sites and the minimum interaction energies with the structures of BRAF, MEK1, MEK2, BRAF-MEK1, and BRAF-MEK2 molecular docking was conducted. Tra was also employed as a MEK1/2 inhibitor to compare with the effects of Xn.

Protein preparation

The X-ray crystallography data of the target proteins, including the BRAF-MEK1 complex, MEK1, and MEK2 from humans (protein data bank (PDB) IDs of 4MNE (6), 4ARK (12), and 1S9I (2)), were obtained from the PDB (available at www.rcsb.org). Additionally, the BRAF-MEK2 complex using B, C, F, and G chains of human BRAF (PDB ID of 4MNE) and MEK2 (PDB ID of 1S9I) were prepared with the help of the HADDOCK2.2 web server (available at <https://milou.science.uu.nl/services/HADDOCK2.2/haddockserver-easy.html>) (13). Finally, following the addition of polar hydrogen atoms to the proteins and the removal of water molecules using the Kollman charge method in Swiss-PDBViewer 4.1 (14).

Ligand preparation

For ligand preparation, the 3-dimensional structures of Xn and Tra (the control drug) were extracted from the PubChem database (available at <https://pubchem.ncbi.nlm.nih.gov>). The ligands using Gasteiger charges in Chimera software version 1.13.1 were minimized, and bond rotations were identified (15).

Molecular docking

In the MEK1, MEK2, and BRAf-MEK1/2 complexes, hydrogen atoms and charges were added using a mosaic machine. Additionally, Chimera software was used to optimize the orientation of the molecules for optimal ligand binding. Blind docking was performed, and a mesh was determined over the whole protein. After placing the ligand onto the protein, targeted splicing was performed at the binding site. A Lamarckian genetic algorithm (LGA) was employed to calculate grid maps (Table 1) in AutoDock 4.2 software (16), and flexibility studies were conducted on the ligands. The grid dimensions of 556, 33.473, and 33.473 Å along the x, y, and z axes, respectively, provided sufficient space for the ligand to rotate freely during the simulation. The LGA method involved 200 distinct connected calculations, including a maximum of 25,000,000 energy evaluations, a maximum of 27,000 generations, a mutation rate of 0.02, a cross-sectional ratio of 0.80, a cluster tolerance of 2 Å, and a population size of 150.

Finally, the binding free energy (ΔG) with the lowest estimated value (docked energy + torsional free energy - the free energy of the unbound system) was selected within each cluster. The results were analyzed and visualized using Discovery Studio 2016 version 16.0.1 software (17).

MD simulation

Based on the docking results for the determining Xn effects on MEK1 and MEK2 proteins, and complexes, BRAf-MEK1/2-ATP dynamic simulations were conducted, and grid maps were shown in Table 2. A simulation was also performed on Tra to compare with Xn. The ligands were minimized using Gasteiger charges in Chimera software version 1.13.1 and the Amber ff99SB force field.

The GROMACS 2022.1 software was employed for MD simulations using the G43a1 force field and TIP4P model for water molecules. Before running the simulations, the energy minimization on the system was performed under both NVT and NPT conditions. NVT refers to the number (N) of particles in the system, the fixed volume (V) of the system, and temperature (T), NPT refers to

the number (N) of particles in the system, the fixed pressure (P) of system, and temperature (T). In the NVT condition, the system was heated to 300 K over 500 ps, and in the NPT condition, the system was heated to 300 K over 1000 ps, with a time step of 0.001 fs. Non-bond interactions were calculated with a 12 Å cutoff using the Particle Mesh Ewald method. Under NVT and NPT conditions, the Berendsen thermostat and the Parrinello-Rahman barostat were used, respectively (18). Data on root mean square deviation (RMSD), root mean square fluctuation (RMSF), the radius of gyration (RG), protein-protein hydrogen bonds, protein-solution hydrogen bonds, and the secondary structure of the target proteins were collected.

Table 1. The grid box size and number of each complex for molecular docking.

Complex name	Box size (Å)
MEK1-Xn	80 × 80 × 90
MEK1-Tra	80 × 80 × 80
MEK2-Xn	126 × 126 × 126
MEK1-Tra	126 × 126 × 120

Å, Angstrom; Xn, xanthohumol; Tra, trametinib.

Table 2. The grid box size, and number of each complex for molecular dynamics simulation.

Complex name	Box size (Å)*
MEK1	4.3 × 4.3 × 3
MEK1-Xn	4.1 × 4.1 × 2.8
MEK1-Tra	6.46 × 6.46 × 4.57
MEK2	5.37 × 5.37 × 3.80
MEK2-Xn	5.37 × 5.35 × 3.80
MEK2-Tra	5.37 × 5.35 × 3.80
BRAf-MEK1	5.81 × 6.94 × 12.72
BRAf-MEK1-Xn	5.81 × 6.94 × 19.89
BRAf-MEK1-Tra	5.81 × 6.94 × 12.21
BRAf-MEK2	5.65 × 5.85 × 4.9
BRAf-MEK2-Xn	6.00 × 5.62 × 11.75
BRAf-MEK2-Tra	7.1 × 6.39 × 5.95

Å, Angstrom; Xn, xanthohumol; Tra, trametinib; BRAf, V-Raf murine sarcoma viral oncogene homolog B1.

RESULTS

Protein and ligand interaction

The results of the docking experiment of Xn (Fig. 1A) and Tra (Fig. 1B) as a control drug with MEK1 and MEK2 proteins as well as with the complexes of BRAf-MEK1 and BRAf-MEK2 modeled by the HADDOCK server were presented in Table 3. According to the results, Xn exhibited the highest binding affinity for MEK1 (-10 Kcal/mol).

The interaction involved 2 hydrogen bonds with the nitrogen atoms of the amino acids Met219 and Asp208. In the interaction with MEK2, the acidic residue of Xn formed 4 hydrogen bonds with the nitrogen atoms of Asn82, Gly83, Ser222, and His104 (Fig. 1C-1F). Notably, regardless of the simulation results, molecular docking demonstrated that the energy score of Xn with the studied proteins closely matched the binding energy of Tra-protein complexes, using the threshold of the control drug (Tra).

MD simulation

To understand the structural changes induced by Xn on MEK1, MEK2, BRaf-MEK1, and BRaf-MEK2 as well as to compare them with the effects of Tra on these proteins, MD simulations were conducted for each protein over a 12 ns time scale. During the simulation, the various parameters, including RMSF, RMSD, energy parameters, RG, the total number of intramolecular hydrogen bonds, and secondary protein structures in the presence of Xn were analyzed. The results were compared with the Tra cases (Table 4).

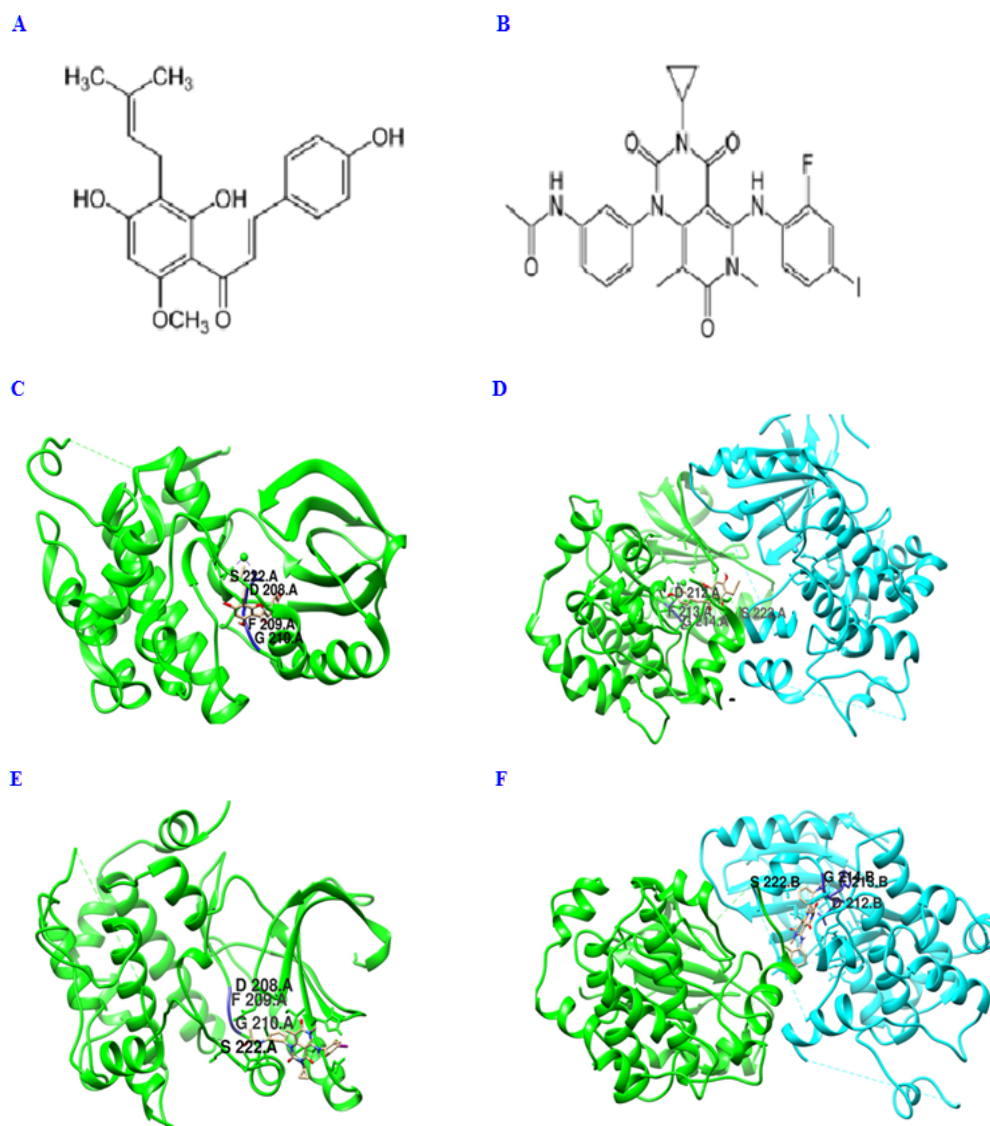


Fig. 1. Two-dimensional structures of Xn and Tra and their interactions with MEK1 and MEK2 proteins highlighting the DFG motif. (A) two-dimensional structure of Xn; (B) two-dimensional structure of Tra; (C) interaction of MEK1 with Xn; (D) interaction of MEK2 with Xn; (E) interaction of MEK1 with Tra; (F) interaction of MEK2 with Tra. Blue segment, DFG motif including aspartate, phenylalanine, and glycine; Xn, xanthohumol; Tra, trametinib.

Table 3. Docking results of Xn and Tra as ligands with MEK1/2-ATP and MEK1/2-ATP-BRaf.

Protein name	Ligand											
	Xn						Tra					
	Energy of bond (Kcal.mol ⁻¹)	Ki (nM)	No. of H-bond	Van der waals	Pi-Pi	Amino acid interacting	Energy of bond (Kcal.mol ⁻¹)	Ki (nM)	No. of H-bond	Van der waals	Pi-Pi	Amino acid interacting
MEK1	-10.70	14.31	2	17	1	Asn78, Met219, Il216, Leu215, Val219, Leu218, Lys97, Met143, Asp208, Ile141, Phe209, Gly210, Ilu99, His188, Arg189, Asp190, Arg234, Met230, Asn221, Ser222,	-11.35	4.75	4	5	0	Ser222, Asn221, Asn78, Leu101, Ser218, Ile103, His100, Glu102, Ile99, Glu79, Met219
BRaf-MEK1-ATP	-10.91	10.09	1	17	0	Arg662, Arg189, Asp190, Asp208, Val127, Cys207, Met143, Phe209	-7.99	0.001	3	17	0	Gln216, Ser216, Phe223, Val224, Arg227, Asn78, Gly77, Gly225, Thr226, Asp901 Pro329, Pro330, Pro33, Pro269, Glu328, Pro334, Arg281,
MEK2	-9.41	126.48	4	10	0	Met223, Lue105, Ile103, Glu106, Asn82, Gly83, Ser222, Ala80, Gly81, Gly84, Val85, His104, Gly83, Met223(B), Ala80(B), Gly84(B), Gly80(B), Gly81(B)	-9.52	14.40	0	9	0	Leu275, Ala272, Pro270, Asp271, Tyr324
BRaf-MEK2-ATP	-8054	0.553	1	16	0	Asp194, Met223, Gly214, Ile220, Leu219, Leu122, Phe213, Phe133, Asp212, Ile145, Ile103, Lys101, Arg193, Val 215, Val131	-8.64	0.465	0	16	0	Glu261, Gln157, Arg662, Ile107, Glu106, Asn660, Ile659, Ile665, Lys160, Leu618, Ser616, Try619, Ile617

Xn, Xanthohumol; Tra, trametinib; BRaf, V-Raf murine sarcoma viral oncogene homolog B1.

Table 4. The values of RMSD, RG, RMSF, and SASA, the number of H bonds, and total energy in MEK1/2-Xn, MEK1/2-Tra, BRaf-MEK1/2-Xn, and BRaf-MEK1/2-Tra.

Complex	RMSD (nm)	RG (nm)	RMSF (nm)	SASA (nm ²)	H-bond between protein-protein	H-bond between protein-solvation	Total energy
MEK1	0.31 ± 0.07	1.97 ± 0.01	0.14 ± 0.08	177.72 ± 1.09	208.03 ± 0.07	618 ± 0.08	-1103663.4 ± 2857.96
MEK1-Tra	0.30 ± 0.06	1.97 ± 0.01	0.12 ± 0.07	177.54 ± 1.10	208.16 ± 0.06	604.40 ± 0.12	-2449658 ± 201166.2
MEK1-Xn	0.34 ± 0.16	2.03 ± 0.05	0.18 ± 0.10	176.54 ± 1.10	210.23 ± 0.07	596.28 ± 0.16	-415151 ± 30862.38
MEK2	0.29 ± 0.01	2.65 ± 0.01	0.13 ± 0.06	364.02 ± 1.94	403.29 ± 0.06	1349 ± 0.13	-939101.31 ± 2062.17
MEK2-Tra	0.28 ± 0.06	1.79 ± 0.01	2.07 ± 0.73	364.01 ± 1.9	412.64 ± 0.09	1324 ± 0.21	-1057832 ± 76273.78
MEK2-Xn	0.34 ± 0.08	2.66 ± 0.02	1.36 ± 0.57	365.50 ± 2.01	406.55 ± 0.10	1330.29 ± 0.19	-1014368 ± 30999.45
BRaf-MEK1	0.48 ± 0.08	5.63 ± 0.03	0.22 ± 0.07	1317.76 ± 3.2	1636.21 ± 0.1	4519.40 ± 0.63	-4435954.62 ± 4199.038
BRaf-MEK1-Tra	0.5 ± 0.13	5.80 ± 0.04	0.24 ± 0.06	1320.54 ± 3.1	1628 ± 0.17	4406.43 ± 0.47	-6073173 ± 470748.5
BRaf-MEK1-Xn	0.5 ± 0.10	5.7 ± 0.04	0.26 ± 0.06	1317052 ± 2.9	1604 ± 0.12	4492.41 ± 0.25	-5150668 ± 104684
BRaf-MEK2	0.37 ± 0.05	5.64 ± 0.01	0.25 ± 0.09	1316.68 ± 1.8	1317.52 ± 2.9	4353.7 ± 0.14	-1338778.9 ± 3099.05
BRaf-MEK2-Tra	0.91 ± 0.02	6.06 ± 0.29	0.63 ± 0.006	1002.03 ± 2.91	1316.68 ± 1.8	3562.19 ± 0.23	-3371153 ± 3563.41
BRaf-MEK2-Xn	0.8 ± 0.17	5.9 ± 0.08	0.30 ± 0.11	1001.98 ± 2.7	1145.08 ± 0.15	3588.05 ± 0.34	-3372494 ± 5919.473

The data of RMSD, RG, RMSF, and SASA were presented as mean ± SD. The data of H bonds and total energy were expressed as mean ± SEM. Xn, Xanthohumol; Tra, trametinib; BRaf, V-Raf murine sarcoma viral oncogene homolog B1; RMSD, root mean square deviation, RMSF, root mean square fluctuation, RG, radius of gyration; SASA, solvent-accessible surface area.

RMSD

To examine the structural stability and the movements of ligand-receptor complexes during the MD simulation, carbon-alpha-RMSD, which was a suitable parameter for evaluating protein stability over time was computed and analyzed (19). Figure 2A shows that the RMSD of the MEK1/2 proteins, MEK1/2-Xn, and MEK1/2-Tra remained stable throughout the simulation. The RMSD of the MEK1-Xn complex initially exhibited an unstable dynamic structure but stabilized at 12000 ps. Figure 2B shows that the complexes of BRaf-MEK1/2-Xn and BRaf-MEK1-Tra achieved structural stability at 6000 ps during the simulation. The BRaf-MEK2-Tra complex displayed structural instability between 6000 and 8000 ps, but achieved relative structural stability between 8000 and 12000 ps (Table 4).

RMSF

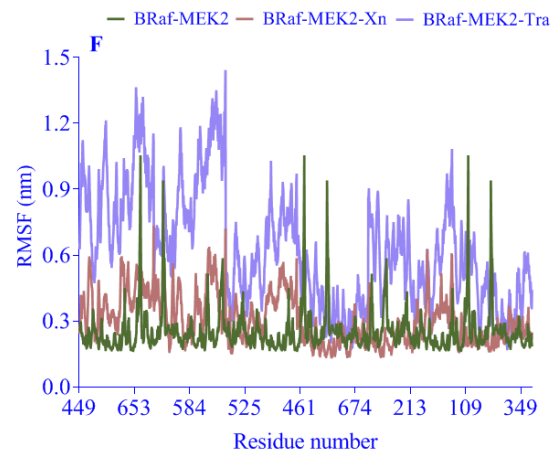
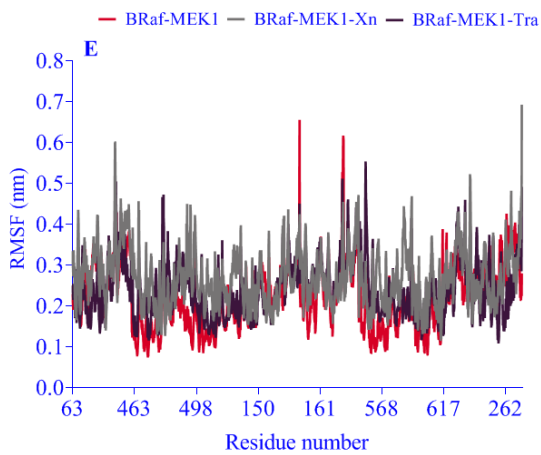
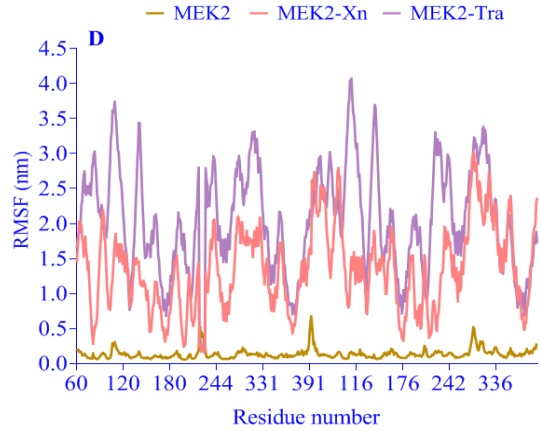
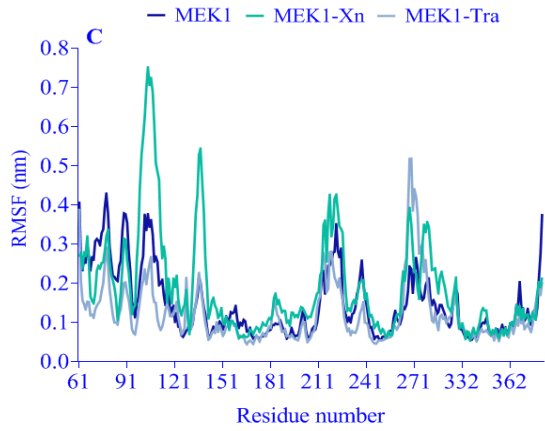
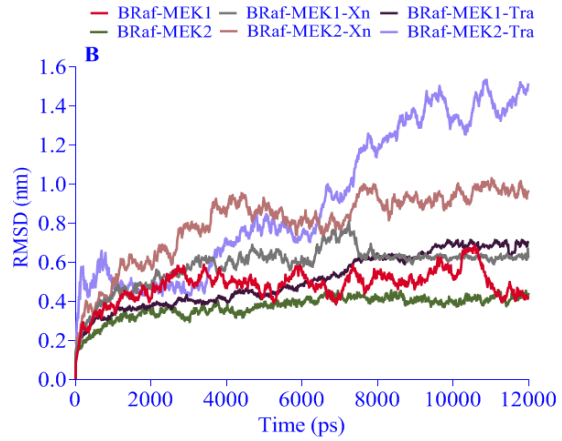
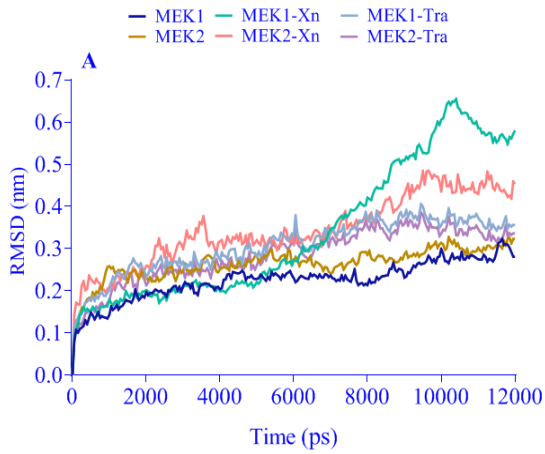
To investigate the effect of Xn on the dynamic behavior of each amino-acid residue and compare it with that of Tra on the amino acids of the studied complexes, the RMSF parameter was calculated (Fig. 2C-2F). Table 4 presents the mean RMSF values in the studied complexes, including MEK1-Xn, MEK1-Tra, MEK2-Xn, MEK2-Tra, BRaf-MEK1-Xn, BRaf-MEK1-Tra, BRaf-MEK2-Xn, and BRaf-MEK2-Tra as well as MEK1/2- and BRaf-MEK1/2-backbones. Structural regions important for kinase activity characteristics were evaluated, and their fluctuations were compared. Based on the results, fluctuations in the catalytic regions of MEK1-Xn and MEK2-Xn were determined to be 0.24 nm and 1.27 nm, respectively. These fluctuations increased compared to the fluctuations in the catalytic region of the MEK1-backbone (0.13 nm) and MEK2-backbone (0.24 nm) in the absence of Xn. The mean oscillations in the catalytic region of MEK1 in the presence of Tra (0.24 nm) were less than those in the presence of Xn, indicating a greater effect of Xn in this region than the control drug. RMSF for the MEK2-Tra region was measured at 2.52 nm,

indicating an increase compared to its value in the presence of Xn. RMSF was assessed in the proline-rich region where BRaf is bound to MEK1/2. According to the results, the average fluctuations of this region in the presence of Xn in MEK1 and MEK2 were 0.25 and 1.39 nm, respectively, while in the absence of Xn, they were 0.21 and 0.14 nm, respectively. The RMSF of this region in the presence of Tra was 0.4 nm (MEK1-Tra) and 2.12 nm (MEK2-Tra) (Fig. 2C and 2D). The fluctuations in the proline-rich region in the BRaf-MEK1/2-Xn complexes were higher compared to MEK1/2, indicating the effect of Xn on these complexes (Fig. 2E and 2F).

RG

To gauge the volume of the MEK1/2 proteins and the BRaf-MEK1/2 complexes under the influence of Xn and to compare it with the Tra the RG of the proteins was examined. Figure 2G shows the changes in the RG of MEK1 and MEK2 proteins in the presence of Xn and the control drug, Tra, at 12000 ps. The mean value of the RG for MEK1 and MEK2 proteins in complex with Xn was 2.03 ± 0.05 and 2.66 ± 0.02 nm, respectively, while this quantity reduced to 1.97 ± 0.01 and 1.79 ± 0.01 nm for MEK1 and MEK2 proteins in complex with Tra, respectively. This implied that Xn could increase the volume of proteins compared to Tra.

According to Fig. 2H, the mean value of the RG of BRaf-MEK1 and BRaf-MEK2 complexes under the influence of Xn was 5.70 ± 0.04 and 5.90 ± 0.08 nm, respectively, while the mean value of the RG of these complexes in the presence of Tra was 5.80 ± 0.04 and 6.06 ± 0.29 nm, respectively. This study also investigated the RG of MEK1 and MEK2 proteins, which were 1.97 and 2.65 nm, respectively. The RG of the MEK1-Xn complex increased compared to MEK1 (Table 4). Table 4 reveals that the RG of the BRaf-MEK1/2-Xn complexes increased compared to the BRaf-MEK1/2 complexes.



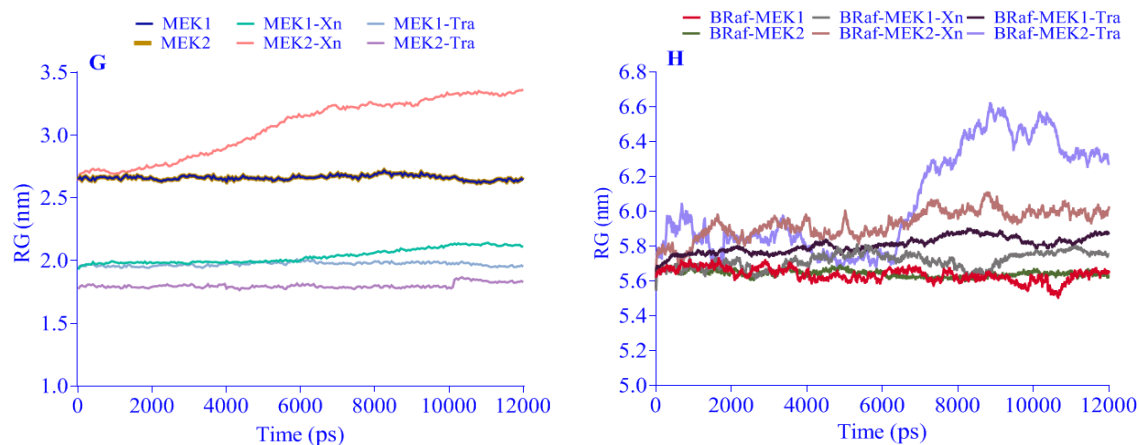


Fig. 2. Molecular dynamics simulation. (A) RMSD of MEK1/2-backbone, MEK1/2-Xn, and MEK1/2-Tra; (B) RMSD of BRaf-MEK1/2-backbone, BRaf-MEK1/2-Xn, and BRaf-MEK1/2-Tra; (C) RMSF of interaction between MEK1-Xn and MEK1-Tra; (D) RMSF of interaction between MEK2-Xn and MEK2-Tra; (E) RMSF of interaction between BRaf-MEK1-Xn and BRaf-MEK1-Tra; (F) RMSF of interaction between BRaf-MEK2-Xn and BRaf-MEK2-Tra; RG plot of protein-backbone of (G) MEK1/2-Xn, MEK1/2-Tra; (H) BRaf-MEK1/2-Xn and BRaf-MEK1/2-Tra. Xn, Xanthohumol; Tra, trametinib; BRaf, V-Raf murine sarcoma viral oncogene homolog B1; RMSD, root mean square deviation, RMSF, root mean square fluctuation, RG, radius of gyration; SASA, solvent-accessible surface area.

Secondary structure

The dictionary of secondary structure of proteins (DSSP) algorithm calculates the most probable assignment of secondary structure based on the 3-dimensional structure of the protein. In this study, the secondary structures of proteins affected by Xn were tested *via* DSSP. To confirm the effect of this ligand on the secondary structure of the proteins it was compared with the results obtained from the activity of Tra on these proteins. Changes in the secondary structure of MEK1/2-Xn complexes compared with MEK1/2-Tra and MEK1/2-backbone were investigated. According to Fig. 3A-3F, in the activation site area of MEK1 (residue numbers: 208-233) in the presence of Xn, the alpha-helix structure was converted to a bend, resembling the structure of the MEK1-Tra complex. These structural changes were also observed in the activation segment of the MEK2 protein (residue numbers: 212-237).

The mean presence probability of the stable alpha-helix and β -strand structures in Xn was 0.11 and 0.15, respectively, and both of them were 0.15 in the presence of Tra. In addition, the values for the unstable structure of bend and turn in MEK2 were 0.1 and 0.12 in the presence of Xn, respectively, and 0.1 and 0.13 in the presence of Tra, respectively (Fig. 3G). Figure 3G shows that the probability of the presence of

the helix element in the MEK1/2-backbone was 0.31 and 0.27, respectively, which was higher than the secondary structure of the alpha-helix in MEK1/2-Xn. This indicated a secondary restructuring in the presence of the ligand.

DISCUSSION

In silico studies represent a prominent contribution in drug design, evaluation, and the predictive interpretation of clinical findings. Bioinformatics studies have gained significance with the development of software and databases for managing large volumes of data, enabling the rapid prediction of target proteins for potential drugs (11). Targeted therapy has opened the door to introducing new drugs for treating various types of cancer by precisely targeting specific proteins involved in the growth and survival of cancer cells. In recent years, there has been a notable increase in the development of MEK inhibitors, and their clinical use has rapidly been growing. Inhibiting the MEK protein, a critical component of the MAPK signaling pathway can be highly effective in blocking this pathway (20). Many studies have confirmed the anticancer effect of Xn on various cancer cells, but there are few studies on the functional activity of Xn on these cells (21).

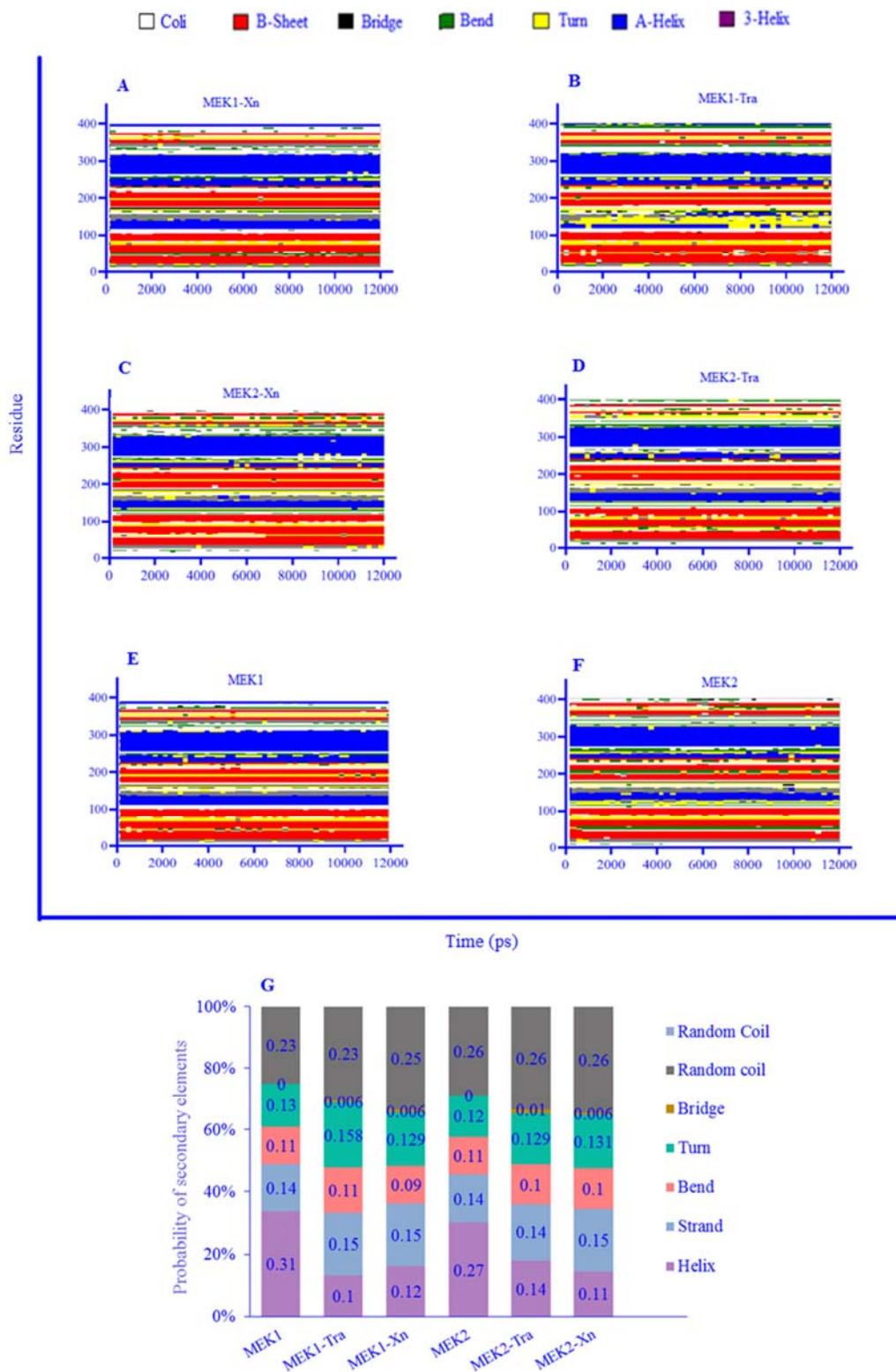


Fig. 3. Time evolution of the secondary structural elements of (A) MEK1-Xn; (B) MEK1-Tra; (C) MEK2-Xn; (D) MEK2-Tra; (E) MEK1-backbone; (F) MEK2-backbone; (G) probability of secondary structures elements in MEK1/2-Xn, MEK1/2-Tra and MEK1/2-backbone. Xn, Xanthohumol; Tra, trametinib.

MEK1 and MEK2 proteins which are the key components of the MAPK pathway were studied as targets in the present study. To better understand the effect of Xn on the BRaf binding site in MEK1/2 the interactions of Xn with the BRaf-MEK1/2 complexes were evaluated. Previous evidence has suggested the involvement of BRaf and MEK in the progression of various cancers (22). BRaf activates MEK through phosphorylation by binding to the proline-rich region of this protein (23). Therefore, this study investigated the BRaf-MEK1/2-Xn complexes to comprehend how Xn might affect MEK inactivation by BRaf. Molecular docking analysis showed that the binding energy of Xn with the studied proteins closely resembled the binding energy of Tra-MEK1/2 complexes. A previous study examined the molecular docking of Xn with kinases in the MAPK/ERK pathway and found the strongest binding energy between Xn and MEK1/2 (24). To determine whether Xn acts as an ATP-competitive or ATP-noncompetitive inhibitor in MEK1 and MEK2, the interactions of the amino acids in these proteins with ATP in the presence and absence of Xn were studied. The docking results for ATP with MEK1 indicated interactions with amino acids such as Asp208, Lys97, Val82, Ala76, Ser194, Gly77, Asn195, Lys192, Asp190, Asn78, Met219, Asn221, Ala220, Ser222, Arg234, His188, Ile216, Arg189, Gly210, and Phe209. Hashemzadeh *et al.* showed that the amino acids including Thr228, Asn78, Lys97, Ser194, and Lys192 in MEK1 interact with ATP (25). Similarly, in another study, Zhu *et al.* reported that the amino acids Lys97, Ala76, Val82, and Asp208 were involved in ATP interactions (26). The present study also revealed that Xn, as a small molecule, interacted with the amino acid residues of the ATP binding site (Fig. 4). Additionally, Xn interacted with the amino acid Ser222, a key amino acid in MEK1 and MEK2 (Fig. 4), which activates MEK1/2 by phosphorylation from BRaf kinase (27,28). The results of the molecular docking simulation revealed very high protein fluctuations in the presence of Xn, particularly in amino acid residues between Ser212 and Gly225, located in the catalytic and activation loops of MEK1 (29). Notably, fluctuations in this region could impact the bonds between this region and ATP.

The findings also highlighted the dependency of RMSF on a range of selected residues in the MEK2-Xn and MEK2-Tra complexes. In Xn, as with Tra, significant fluctuations were observed in the A and B chains of MEK2, with a notable RMSF in the amino acid Ser222 pivotal in MEK2. Moreover, amino acids like Lys63, Gly65, Leu389, and Arg388 exhibited high volatility in positions 266 to 334, a region rich in prolines associated with the BRaf binding site (30,23). This fluctuation pattern indicated that Xn, much like Tra, could potentially inhibit MEK1 and MEK2 by hindering their phosphorylation by BRaf, consistent with previous research (31). Liu *et al.* demonstrated that Xn decreased MEK phosphorylation in the HT-29 cell line a colon cancer cell line (31). In another study, Gao *et al.* reported that Xn reduces ERK1/2 phosphorylation, confirming the current findings that Xn might decrease ERK1/2 phosphorylation by inhibiting upstream kinases such as MEK1/2 (32).

Protein interactions are often associated with significant changes in composition, which can be assessed through the RG, providing insight into protein structural compactness (33). The present study showed that Xn could increase the volume of proteins compared to Tra consistent with the observed changes in RG in BRaf-MEK1 and BRaf-MEK2 complexes influenced by Xn and Tra. These results can be related to protein structure. Moreover, these results are consistent with the solvent-accessible surface area (SASA), an important factor in protein structural changes. SASA is defined as a hypothetical center of a solvent sphere with the van der Waals contact molecule surface as the surface characterized around a protein (34). As a ligand, Xn was found to induce denaturation in MEK1/2 proteins and BRaf-MEK1/2 complexes, exposing the hydrophobic region to solvent when the proteins were unfolded (35). Like Tra, these findings supported the idea that Xn could make these proteins permeable and accessible to water molecules. In confirming the current findings, demonstrating the inhibitory effect of Xn on MEK1 and MEK2 proteins, Festa *et al.* showed that Xn plays an important role in cell death by affecting the MAPK pathway (36). In another study, Seitz *et al.* showed that Xn inhibited melanoma cell growth and had an anti-metastatic effect (21).

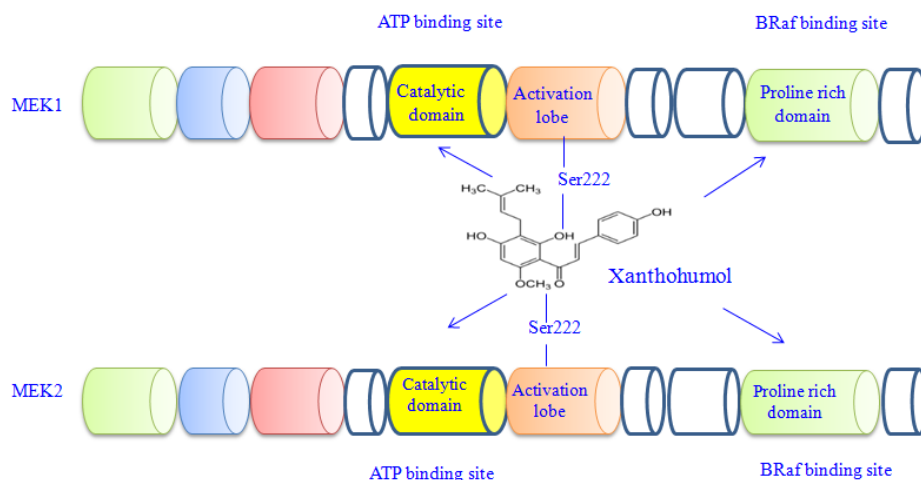


Fig. 4. Interaction between Xn and MEK1/2 in 3 regions of MEK1/2 (catalytic activation and proline-rich domains)

One of the signs of stability and strength in chemical compounds is the formation of hydrogen bonds (37). The present results indicated that Xn, like the control drug Tra, could affect the structure of the target proteins in this study, leading to increased hydrogen bonds between the target proteins and the solvent; ultimately reducing protein stability (38).

The examination of secondary structures showed that Xn, similar to Tra, influenced the presence of flexible turn and bend structures in the studied proteins, making the protein structure more flexible by introducing these structures between the stable alpha-helix and beta-strands. These alterations suggested a potential modification in the protein structure by the drug.

The analysis of protein flexibility over time, as seen through DSSP analysis for secondary structure, indicated that both MEK1 and MEK2 structures became unstable and degraded in the presence of Xn, similar to the results observed with Tra. Notably, MEK1/2 contains a glycine-rich amino acid loop that increases the flexibility of the protein structure. This glycine-rich loop is associated with a β -strand structure that overlaps the ATP-binding site. The flexibility of this loop is required for the connection of ATP to the binding site and ADP release in each cycle (31).

The results showed that the amino acids at the ATP-binding site formed a secondary β -strand structure. Many of these amino acids bend and turn secondary structures in the

presence of Xn. A range of important and key amino acids, involved in the activation of the MEK1 protein, formed the bend and turn structures due to the interaction of MEK1 with Xn. These amino acids were Ile216, Met219, and Asn219, present at the ATP binding site in MEK1. The other two important amino acids were Ser222 and Ser218 in the catalytic site of the MEK1 protein whose phosphorylation by BRaf led to the activation of MEK1.

The results showed that these amino acids caused instability in the MEK1 protein structure by creating turn and bend structures. This pattern of secondary structure in the MEK1-Xn complex was similar to the secondary structure in MEK1 in the presence of Tra. Irregular secondary structures of bend and turn were observed at the ATP binding site in MEK2. Therefore, it might affect the ATP binding to MEK2. Similar to MEK1, MEK2 was activated by the phosphorylation of Ser222. Ser222 was also involved in the formation of turn and bend secondary structures in the presence of Xn. These structures were also seen in the presence of Tra in MEK2. The pattern of the secondary structures in MEK2 in the presence of Xn and Tra was very similar. Elements of the secondary structure of the proteins can help introduce a new drug (39). Although we conducted this research with low simulation time based on the existence of reports with a similar approach, it is still advisable to increase simulation this time to further assess the stability of the protein-ligand complex.

CONCLUSION

This computational study showed that Xn could affect MEK1/2. The effect of Xn on MEK1 and MEK2, B Raf-MEK1, and B Raf-MEK2 complexes could be viewed as an advantageous outcome. Xn inhibited the phosphorylation and activation of MEK1/2 by affecting the catalytic and ATP-binding domains of the proteins. Xn might also impact the functionality of B Raf by influencing the structure of the proline-rich MEK1/2 region. Consequently, this study strongly supported the idea that targeting MEK1 and MEK2 proteins with Xn can be a promising strategy for inhibiting the MAPK pathway.

Acknowledgments

The authors are grateful to Mrs. Hajipour for her English-language comments on the initial draft of the manuscript. We also thank Dr. Elaheh Kashani-Amin, Dr. Yazdan Asgari, Dr. Ali Salehzadeh-Yazdi, and Dr. Shohreh Gholizadeh Siahmazgi for their helpful suggestions and advice.

Conflict of interest statement

The authors declare that they have no conflict of interest.

Authors' contributions

Z. Gholizadeh Siahmazgi developed the tools, collected and analyzed the data, interpreted the results, and prepared the draft of the first manuscript; S. Irani analyzed the data and interpreted the results; A. Ghiaseddin developed the tools and interpreted the results; F. Soutodeh, Z. Gohari, J. Afifeh, and A. Pashapouryeganeh collected the data and interpreted the results; H. Samimi analyzed the data and interpreted the results; M. Naderi and P. Fallah developed the tools, collected and analyzed the data, and interpreted the results; V. Haghpanah conceptualized and supervised all aspects of the work. All authors critically reviewed and approved the final draft of the manuscript.

REFERENCES

1. Akinleye A, Furqan M, Mukhi N, Ravella P, Liu D. MEK and the inhibitors: From bench to bedside. *J Hematol Oncol.* 2013;6(27):1-11. DOI: 10.1186/1756-8722-6-27.
2. Ohren JF, Chen H, Pavlovsky A, Whitehead C, Zhang E, Kuffa P, *et al.* Structures of human MAP kinase kinase 1 (MEK1) and MEK2 describe novel noncompetitive kinase inhibition. *Nat Struct Mol Biol.* 2004;11(12):1192-1197. DOI: 10.1038/nsmb859.
3. McCubrey JA, Steelman LS, Chappell WH, Abrams SL, Wong EWT, Chang F, *et al.* Roles of the Raf/MEK/ERK pathway in cell growth, malignant transformation and drug resistance. *Biochim Biophys Acta.* 2007;1773(8):1263-1284. DOI: 10.1016/j.bbamcr.2006.10.001.
4. Wright CJM, McCormack PL. Trametinib: first global approval. *Drugs.* 2013;73(11):1245-1254. DOI: 10.1007/s40265-013-0096-1.
5. Patel M, Eckburg A, Gantiwala S, Hart Z, Dein J, Lam K, *et al.* Resistance to molecularly targeted therapies in melanoma. *Cancers (Basel).* 2021;13(5):1-25. DOI: 10.3390/cancers13051115.
6. Caunt CJ, Sale MJ, Smith PD, Cook SJ. MEK1 and MEK2 inhibitors and cancer therapy: the long and winding road. *Nat Rev Cancer.* 2015;15(10):577-592. DOI: 10.1038/nrc4000.
7. Cheng Y, Tian H. Current development status of MEK inhibitors. *Molecules.* 2017;22(10):1-20. DOI: 10.3390/molecules22101551.
8. Jiang CH, Sun TL, Xiang DX, Wei SS, Li WQ. Anticancer activity and mechanism of xanthohumol: a prenylated flavonoid from hops (*Humulus lupulus L.*). *Front Pharmacol.* 2018;9(530):1-13. DOI: 10.3389/fphar.2018.00530.
9. Gholizadeh Siahmazgi Z, Irani S, Ghiaseddin A, Fallah P, Haghpanah V. Xanthohumol hinders invasion and cell cycle progression in cancer cells through targeting MMP2, MMP9, FAK and P53 genes in three-dimensional breast and lung cancer cells culture. *Cancer Cell Int.* 2023;23(1):153,1-11. DOI: 10.1186/s12935-023-03009-2.
10. Lee S, Rauch J, Kolch W. Targeting MAPK signaling in cancer: mechanisms of drug resistance and sensitivity. *Int J Mol Sci.* 2020;21(3):1102,1-29. DOI: 10.3390/ijms21031102.
11. Wishart DS. Bioinformatics in drug development and assessment. *Drug Metab Rev.* 2005;37(2):279-310. DOI: 10.1081/dmr-55225.
12. Hartung IV, Hitchcock M, Pühler F, Neuhaus R, Scholz A, Hammer S, *et al.* Optimization of allosteric MEK inhibitors. Part 1: venturing into underexplored SAR territories. *Bioorganic Med Chem Lett.* 2013;23(8):2384-2390. DOI: 10.1016/j.bmcl.2013.02.028.
13. Isfahani MB, Mahnam K, Seyedhosseini-Ghaheh H, Sadeghi HMM, Khanahmad H, Akbari V, *et al.* Computational design of newly engineered DARPins as HER2 receptor inhibitors for breast cancer treatment. *Res Pharm Sci.* 2023;18(6):626-637. DOI: 10.4103/1735-5362.389950.
14. Johansson MU, Zoete V, Michielin O, Guex N. Defining and searching for structural motifs using DeepView/Swiss-PdbViewer. *BMC Bioinformatics.* 2012;13:173,1-10. DOI: 10.1186/1471-2105-13-173.
15. Hashemi-shahraki F, Shareghi B, Farhadian S. The interaction of naphthol yellow S (NYS) with pepsin:

- insights from spectroscopic to molecular dynamics studies. *Int J Biol Macromol.* 2020;165:1842-1851. DOI: 10.1016/j.ijbiomac.2020.10.093.
16. Rajaei N, Rahgouy G, Panahi N, Razzaghi-Asl N. Bioinformatic analysis of highly consumed phytochemicals as P-gp binders to overcome drug-resistance. *Res Pharm Sci.* 2023;18(5):505-516. DOI: 10.4103/1735-5362.383706.
 17. Tannas LE. System requirements. In: Flat-panel displays and CRTs. 1th ed. Dordrecht: Springer; 1985.pp. 31-53. DOI: 10.1007/978-94-011-7062-8_2.
 18. Messias A, Santod DES, Pontes FJS, Lima FS, Soares TA. Out of sight, out of mind: the effect of the equilibration protocol on the structural ensembles of charged glycolipid bilayers. *Molecules.* 2020;25(21):1-16. DOI: 10.3390/molecules25215120.
 19. Hatami S, Sirous H, Mahnam K, Najafipour A, Fassihi A. Preparing a database of corrected protein structures important in cell signaling pathways. *Res Pharm Sci.* 2022;18(1):67-77. DOI: 10.4103/1735-5362.363597.
 20. Han J, Liu Y, Yang S, Wu X, Li H, Wang Q. MEK inhibitors for the treatment of non-small cell lung cancer. *J Hematol Oncol.* 2021;14(1):1,1-12. DOI: 10.1186/s13045-020-01025-7.
 21. Seitz T, Hackl C, Freese K, Dietrich P, Mahli A, Thasler RM, *et al.* Xanthohumol, a prenylated chalcone derived from hops, inhibits growth and metastasis of melanoma cells. *Cancers (Basel).* 2021;13(3):1-12. DOI: 10.3390/cancers13030511.
 22. Roberts PJ, Der CJ. Targeting the Raf-MEK-ERK mitogen-activated protein kinase cascade for the treatment of cancer. *Oncogene.* 2007;26(22):3291-3310. DOI: 10.1038/sj.onc.1210422.
 23. Catling AD, Schaeffer HJ, Reuter CW, Reddy GR, Weber MJ. A proline-rich sequence unique to MEK1 and MEK2 is required for raf binding and regulates MEK function. *Mol Cell Biol.* 1995;15(10):5214-5225. DOI: 10.1128/mcb.15.10.5214.
 24. Gholizadeh Siahmazgi Z, Irani S, Ghiaseddin A, Fallah P, Haghpanah V. Bioinformatic study on effect of xanthohumol as bioactive compound of HOP in the inhibition of the MAPK/ERK pathway in thyroid cancer. *Iran J Diabetes Metab.* 2020;19(4):225-233.
 25. Hashemzadeh S, Ramezani F, Rafii-Tabar H. Study of molecular mechanism of the interaction between MEK1/2 and trametinib with docking and molecular dynamic simulation. *Interdiscip Sci Comput Life Sci.* 2019;11(1):115-124. DOI: 10.1007/s12539-018-0305-4.
 26. Zhu J, Li C, Yang H, Guo X, Huang T, Han W. Computational study on the effect of inactivating/activating mutations on the inhibition of MEK1 by trametinib. *Int J Mol Sci.* 2020;21(6):2167,1-15. DOI: 10.3390/ijms21062167.
 27. Fleischmann J, Feichtner A, Defalco L, Kugler V, Schwaighofer S, Huber RG, *et al.* Allosteric kinase inhibitors reshape mek1 kinase activity conformations in cells and in silico. *Biomolecules.* 2021;11(4):518,1-13. DOI: 10.3390/biom11040518.
 28. Wu PK, Becker A, Park JI. Growth inhibitory signaling of the raf/mek/erk pathway. *Int J Mol Sci.* 2020;21(15):1-12. DOI: 10.3390/ijms21155436.
 29. Roskoski Jr. MEK1/2 dual-specificity protein kinases: Structure and regulation. *Biochem Biophys Res Commun.* 2012;417(1):5-10. DOI: 10.1016/j.bbrc.2011.11.145.
 30. Roskoski Jr. Allosteric MEK1/2 inhibitors including cobimetanib and trametinib in the treatment of cutaneous melanomas. *Pharmacol Res.* 2017;117:20-31. DOI: 10.1016/j.phrs.2016.12.009.
 31. Liu X, An LJ, Li Y, Wang Y, Zhao L, Lv X, *et al.* Xanthohumol chalcone acts as a powerful inhibitor of carcinogenesis in drug-resistant human colon carcinoma and these effects are mediated via G2/M phase cell cycle arrest, activation of apoptotic pathways, caspase activation and targeting Ras/MEK/ERK pa. *J BUON.* 2019;24(6):2442-2447. PMID: 31983118.
 32. Gao F, Li M, Zhou L, Liu W, Zuo H, Li W. Xanthohumol targets the ERK1/2-Fra1 signaling axis to reduce cyclin D1 expression and inhibit non-small cell lung cancer. *Oncol Rep.* 2020;44(4):1365-1374. DOI: 10.3892/or.2020.7697.
 33. Lobanov Yu, Bogatyreva NS, Galzitskaya OV. Radius of gyration as an indicator of protein structure compactness. *Mol Biol.* 2008;42(4):623-628. DOI: 10.1134/S0026893308040195.
 34. Kim SB, Singh RS, Paul PKC, Debenedetti PG. Effects of disulfide bridges and backbone connectivity on water sorption by protein matrices. *Sci Rep.* 2017;7:7957,1-9. DOI: 10.1038/s41598-017-08561-2.
 35. Malleshappa Gowder S, Chatterjee J, Chaudhuri T, Paul K. Prediction and analysis of surface hydrophobic residues in tertiary structure of proteins. *Sci World J.* 2014;2014:1-7. DOI: 10.1155/2014/971258.
 36. Festa M, Capasso A, D'Acunto CW, Masullo M, Rossi AG, Pizza C, *et al.* Xanthohumol induces apoptosis in human malignant glioblastoma cells by increasing reactive oxygen species and activating MAPK pathways. *J Nat Prod.* 2011;74(12):2505-2513. DOI: 10.1021/np200390x.
 37. Assadollahi V, Rashidieh B, Alasvand M, Abdolahi A, Lopez JA. Interaction and molecular dynamics simulation study of Osimertinib (AstraZeneca 9291) anticancer drug with the EGFR kinase domain in native protein and mutated L844V and C797S. *J Cell Biochem.* 2019;120(8):13046-13055. DOI: 10.1002/jcb.28575.
 38. Pace CN, Fu H, Fryar KL, Landua J, Trevino SR, Schell D, *et al.* Contribution of hydrogen bonds to protein stability. *Protein Sci.* 2014;23(5):652-661. DOI: 10.1002/pro.2449.
 39. Koch O. Use of secondary structure element information in drug design: polypharmacology and conserved motifs in protein-ligand binding and protein-protein interfaces. *Future Med Chem.* 2011;3(6):699-708. DOI: 10.4155/fmc.11.26.